The Impact of Encapsulation on Lithium Transport and Cycling Performance for Silicon Electrodes on Aligned Carbon Nanotube Substrates

Juichin Fan,[a,*] Lawrence K. Barrett,[b] Robert C. Davis,[b] Richard R. Vanfleet,[b] and John N. Harb[a,**,z]

aDepartment of Chemical Engineering, Brigham Young University, Provo, Utah, USA
bDepartment of Physics and Astronomy, Brigham Young University, Provo, Utah, USA

In this study, silicon-coated vertically aligned carbon nanotube (Si-VACNT) electrodes were used to examine the impact of encapsulation, which effectively reduced the surface area exposed to the electrolyte. This system is ideal for examining the influence of an electrolyte-blocking layer due to its well-defined geometry and high aspect ratio. The morphology, composition and electrochemical performance of electrodes cycled at different rates were characterized for a range of silicon loadings. Significant differences were observed in the morphology and composition of the electrodes. However, the electrochemical performance was similar, and capacity fading was still observed for the encapsulated electrodes. The impact of the encapsulation layer on lithium transport was examined. Two different transport directions and length scales are relevant–1) radial transport of Li in/out of each silicon-coated nanotube (∼50 nm diameter) and 2) lithium transport along the length of the nanotubes (∼100 μm height). Experimental results indicate that the height of the Si-VACNT electrodes does not limit Li transport, even though that height was orders of magnitude greater than the diameter of the tubes. These results have important implications for a variety of encapsulation strategies.

In order to enhance the cycle life and energy density of next-generation lithium-ion batteries (LIBs), numerous strategies have been developed that include the use of improved electrode materials and structures. These materials and structures impact cell performance and cycle life by influencing properties such as mechanical stability, the surface area available for reaction, and the transport of reactants and products into and out of the electrodes. For decades, commercial LIBs have used graphite as the anode material of choice. Its advantages include low cost, a moderately high energy density, a low lithiation potential, and a high Li$^+$ diffusivity; however, its specific capacity is relatively low compared to that of alloy-type materials. Silicon, one of the alloy-type materials, stands out as a promising anode candidate due to its high theoretical gravimetric capacity (3,579 mAh/g at room temperature[1]) and its low working potential relative to Li/Li$^+$.[2] Unfortunately, the performance of silicon electrodes has been limited by large volume changes upon cycling (up to 300%[3]) as well as by the formation of an unstable solid-electrolyte interphase (SEI).[4] Volume changes associated with lithiation and delithiation may compromise electrode integrity and result in the loss of contact with the current collector, leading to poor electrode capacity and high rates of cycle fading. Nanostructured electrodes, such as nanostructured silicon[5–8] and core-shell composite electrodes,[9–15] have been shown to accommodate silicon volume changes, at least to some extent. However, the high interfacial area of nano-structured electrodes tends to exacerbate problems associated with SEI formation. As cycling proceeds, continuous electrolyte degradation and consumption of Li ions result in the formation of a thick and unstable SEI layer, increasing the internal resistance and contributing to capacity fade.[16] To date, capacity fading has been attributed to the combined effect of electrode volume changes and SEI formation.

Various nanoscale electrode structures have been utilized, including spheres (nanoparticles) and cylinders (nanowires and nanotubes), to help mitigate the impact of volume changes during the cycling of silicon electrodes. Also, the incorporation of void space inside nanoparticles has been shown to enhance performance relative to solid nanoparticles.[10,17,18] Minimal outward expansion helps to avoid fracturing of the SEI and to maintain a good contact between the active materials and conductive additives. Independent of the specific geometry, conductive additives are important; pure silicon nanospheres or

1-D structures alone are not sufficient for good capacity retention.[19] Core-shell composite electrodes that combine silicon with electrically conductive materials such as graphene, carbon, or carbon nanotubes seek to exploit the merits of each of the materials.
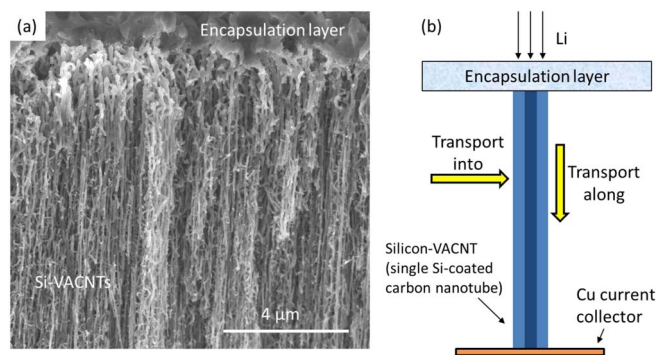
Efforts have also been made to change the interfacial properties or to decrease the interfacial surface area between the electrode and the electrolyte in order to improve stability. Evanoff et al.[15] demonstrated that their ultra-thick (∼1 mm) silicon-coated vertically aligned carbon nanotube (Si-VACNT) electrode protected by a carbon layer over the silicon had a Coulombic efficiency close to 99%, while a similar but unprotected Si-VACNT electrode had a Coulombic efficiency less than 98%. In another study, Liu et al.[18] developed a pomegranate-like design for a silicon electrode by first coating silicon nanoparticles with a conductive carbon layer and then assembling multiple nanoparticles within a second carbon layer to form a hierarchical structure that reduced and stabilized SEI formation. Images taken after cycling showed that the electrolyte-blocking outer carbon layer limited SEI formation. A stable capacity of 1,160 mAh/g at C/2 was observed after 1,000 cycles. A similar type of approach was used by Yi et al.[20] who constructed graphene-wrapped Si–C composite electrodes. The contact area between the Si-C particles and the electrolyte was minimized by the use of graphene layers. The resulting gravimetric capacities of the graphene-wrapped electrodes stayed at approximately 1,100 mAh/g for at least 40 cycles, independent of the silicon loading, while the electrodes without graphene layers experienced significant capacity fading and had low capacities. Capacity fade became more significant as the silicon loading increased. Microscopic images taken after cycling indicated that the graphene sheets were able to maintain a conductive network, even though the underlying Si-C structure fractured. The examples discussed above illustrate the benefits of modifying and reducing the contact area between the electrode and the electrolyte in order to decrease the amount of SEI formed upon cycling while maintaining an adequate conductive network.

In this study, Si-VACNT electrodes were fabricated with use of vertically aligned carbon nanotubes (VACNTs) as a template, which provided direct electronic connection to the current collector, mechanical support for the silicon, and adequate void space to accommodate electrode expansion. The silicon was infiltrated into the carbon nanotube template and deposited directly onto the nanotubes. The resulting Si-VACNT structures enabled control of the electrode height, silicon loading and, to some extent, the contact area between the electrode and

---

*Electrochemical Society Student Member.
**Electrochemical Society Member.
zE-mail: john_harb@byu.edu

Figure 1. (a) SEM micrograph of an encapsulated Si-VACNT electrode and (b) schematic diagram of an individual encapsulated Si-VACNT showing Li transport directions.

the electrolyte. However, the nanostructured-nature of the Si-VACNT electrodes creates a high silicon surface area in contact with the electrolyte unless a protective layer is also fabricated. Consequently, a carbon encapsulation layer was constructed as a barrier to prevent the electrolyte from contacting the silicon, as shown in Figure 1. To the extent that this layer was effective, SEI formation was limited to the more stable interface between the carbon encapsulation layer and the electrolyte.[20] This strategy for electrolyte exclusion, as well as any other similar strategy, precludes the transport of Li-ions through the liquid electrolyte to the silicon. Instead, the lithium must now move along or through the solid Si-VACNT phase to utilize the full capacity of the electrode. The success of electrolyte exclusion from nanostructured silicon depends on the ability to transport lithium into and out of the silicon in the absence of a liquid electrolyte phase. The characteristics of Si-VACNT electrodes, including aligned nanotubes, very high aspect ratios and controllable tube height, offer a unique opportunity to study the impact of encapsulation for electrolyte exclusion on the performance of silicon electrodes. Consequently, this study uses these electrodes to examine the following: 1) the role of the SEI in capacity fade for Si-VACNT electrodes, 2) the factors that limit the performance of encapsulated electrodes, 3) the relative rates of transport along and into the silicon-coated nanotubes, 4) the absolute transport rate of lithium along the nanotubes in the vertical (thickness) direction, and 5) the correlation between the interfacial current density and the capacity of the electrodes under a variety of conditions. Electrochemical characterization and microscopic analysis of electrodes before and after cycling are used to examine these issues.

Experimental

Fabrication of Si-VACNTs.—Vertically aligned carbon nanotubes were synthesized via chemical vapor deposition as described elsewhere.[21] Prior to VACNT growth, a 4 nm thick layer of iron catalyst (99,97%, irregularly shaped, Alfa Aesar) was deposited on substrates via thermal evaporation at 1×10^{-5} *Torr*. Vertically aligned carbon nanotubes were then grown from a gaseous mixture of H_2 and C_2H_4 in a tube furnace (Lindberg/Blue M 1100°C Tube Furnaces, Thermo Scientific). Hydrogen flowed through the furnace at a rate of 232.67 sccm while the furnace was heated to the desired temperature. Once that temperature (750°C) was reached, the flow of ethylene at a rate of 249.3 sccm was initiated. The observed growth rate of VACNTs was approximately 1.3 μm/sec. When the CNT growth was complete, the temperature of the furnace was increased to 900°C for carbon infiltration on the CNTs in order to reinforce their mechanical stability. The carbon infiltration was carried out for one to two minutes, depending on the height and density of the Si-VACNTs. After VACNT fabrication, a KOH etch (30% by mass) was used to detach the VACNT structure from the Si substrate prior to the deposition of silicon onto the carbon nanotubes. Samples were immersed in the KOH solution at ∼75°C for 20 to 30 minutes. VACNT samples were subsequently

soaked in de-ionized water for 10 minutes and then transferred to isopropanol for another 10 minutes. Samples were finally dried overnight at room temperature prior to silicon deposition. Dried samples were then weighed, and at least three measurements of the height of each sample were made with an optical microscope (BX60, Olympus). The resulting mass and the average height were used for calculation of the silicon loading.
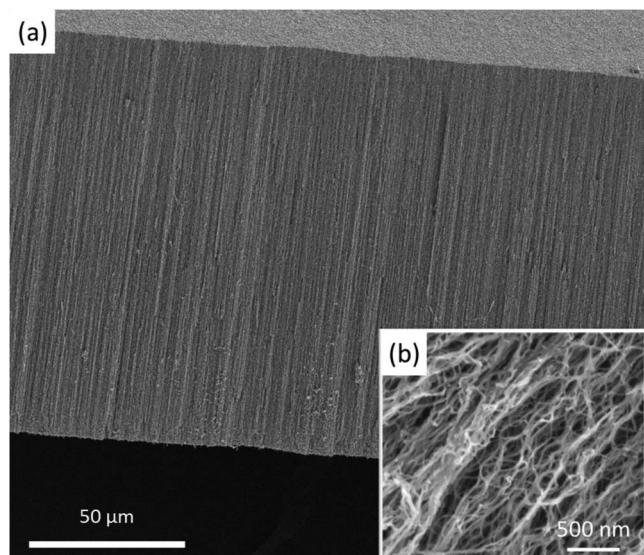
Si deposition was performed by low-pressure chemical vapor deposition (LPCVD) at 200 mTorr and 535°C. Silane (SiH_4) was fed into the tube furnace at a rate of 20 sccm. A variety of Si deposition times, ranging from 10 to 30 min, was used to provide the desired Si loading. The mass of each sample was measured before and after Si infiltration in order to obtain the Si loading. The measured silicon mass was converted to the silicon volume fraction relative to the total volume of an electrode (including void volume). Si-VACNT samples that were not going to be encapsulated were transferred directly to an argon-filled glove box for cell assembly. Those electrodes that required encapsulation were covered and stored to prevent contamination.

CNT/PECVD encapsulation fabrication.—After silicon infiltration, cells were encapsulated as follows. First, carbon nanotubes were sprayed onto the electrode surface to provide a more homogeneous and smooth surface upon which the encapsulation layer could be grown. Without this CNT layer, it would have been very difficult to encapsulate the Si-VACNT electrodes. The spray solution contained multi-walled carbon nanotubes (MWCNTs, Aldrich Sigma) and *N*-Methyl-2-pyrrolidone (NMP) (semiconductor grade, Aldrich Sigma) at a ratio of 1.2 mg CNTs/mL of NMP. The CNT/NMP solution was sonicated and then centrifuged.[22] Only the top two-thirds of the centrifuged solution was used in order to obtain a more uniform size distribution of CNTs. The resulting CNT solution was injected into the nozzle (Impact EDGE Air Shaping System, Sono-Tek) of an ultrasonic sprayer (ECHO ultrasonic generator 250 kHz, Sono-Tek). CNT spraying was carried out at 200°C on a hot plate. Following spray deposition of the CNT layer, an encapsulation layer consisting of approximately 0.12 ± 0.03 mg/cm² of amorphous carbon was deposited by plasma-enhanced CVD (PECVD) at 1 Torr and room temperature from a gaseous mixture of 98% helium and 2% methane (Airgas). Each PECVD run was performed for 45 minutes to ensure complete encapsulation. The very last step in the fabrication process was to deposit a 250 nm layer of copper (Chemical MFG. Corp) on the back side of each sample by thermal evaporation to serve as the current collector.

Electrochemical characterization and microscopy.—Once fabrication was completed, Si-VACNT electrodes with and without the encapsulation layer were assembled into CR2025 coin cells with Li metal disks as the counter electrodes. Two electrolytes were used–1) 1M $LiPF_6$ in 1:1 mixture of ethylene carbonate and diethyl carbonate (EC/DEC), and 2) the same EC/DEC electrolyte with 10% by mass fluoroethylene carbonate (Sigma Aldrich, battery grade). Two layers of Celgard 2400 PP (polypropylene, 25 μm) separator were used in order to avoid lithium dendrite formation that can cause shorting of cells with metallic Li electrodes. The separator layers were soaked in the electrolyte until they were completely wetted prior to assembly. All coin cells were allowed to sit for at least 12 hours after assembly and before testing. Electrochemical cycling was performed using either a MACCOR 4300 or an Arbin BT 2000 battery tester. All cells were cycled in the potential window from 0.05 to 1V vs. Li/Li⁺. The capacity was normalized by the mass of silicon after eliminating the portion of the capacity due to carbon (which was measured to be ∼200 mAh/g for the carbon infiltrated VACNT electrodes).

After cycling, electrode samples were obtained by disassembling cells in an argon-filled glove box. Electrodes were rinsed in ethylene carbonate to remove residual electrolyte. For some electrodes, the SEI was removed by soaking in 99% HCl for one hour and then rinsing with distilled water to remove the acid. All samples were dried and transferred inside aluminum-coated zip-lock bags to the microscopes for examination. Scanning Electron Microscopes (S-Feg
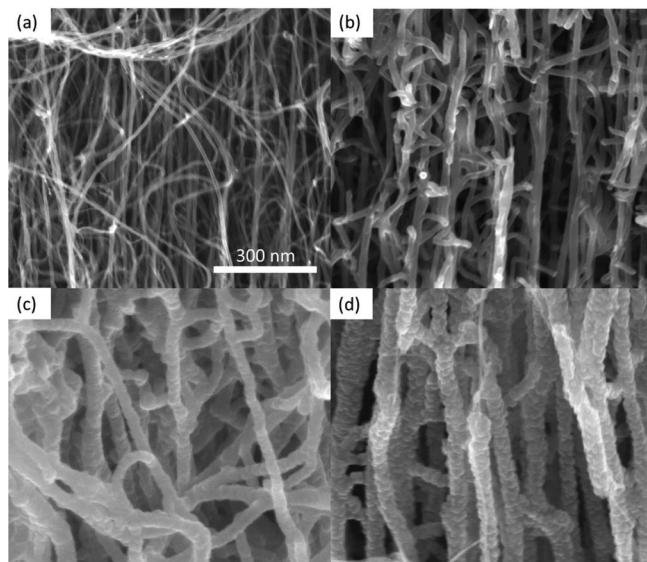
Figure 2. (a) SEM micrograph of VACNT forest cross-section and (b) inset at higher magnification showing tube structure.

XL30 and Helios NanoLab 600 DualBeam FIB/SEM, FEI) were used to examine the morphology and topography of the surface and cross sections; Energy Dispersive X-ray analysis (EDS, 5 kV) was used to measure chemical composition.

Results and Discussion

Nanostructure of Si-VACNTs and the encapsulation layer.—Vertically aligned carbon nanotubes (Figure 2a) provide both enhanced electrical conductivity and robust mechanical support in a controllable, reproducible format. These structures are highly porous on the nanoscale as shown in the in Figure 2b, where carbon nanotubes account for only about one percent of the volume. On average, two minutes of VACNT growth yielded nanotubes that were approximately 135 ± 13 μm high, while growth for one minute resulted in a nanotube height of 70 ± 8 μm. The average diameter of bare CNTs was 11 ± 1 nm (Figure 3a), which is significantly less than the average space between nanotubes ($\sim$100 nm); consequently, these ordered CNT templates allow for carbon and silicon infiltration over a wide range of thicknesses. Regarding the carbon infiltration, the average tube diameter after one minute of infiltration was about 25 ± 2 nm, while the average tube diameter after two minutes was about 40 ± 3 nm (Figure 3b). Figures 3c and 3d show that the silicon formed a uniform layer on the carbon nanotubes with an average tube diameter of 45–50 nm for lightly loaded ($\sim$2%) electrodes and an average tube diameter of 52–67 nm for the heavily loaded ($\sim$10%) electrodes, respectively. Given the dimensions of the height and diameter of Si-VACNTs, the high aspect ratio is evidently an important feature for Li transport.
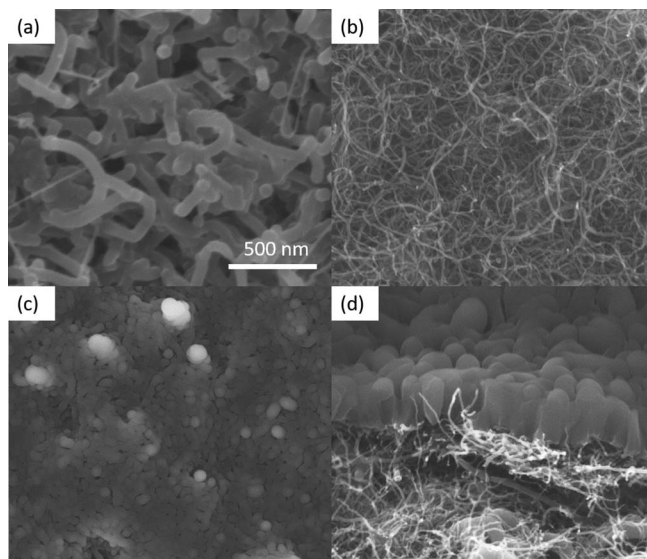
Figure 4 shows the top surface of the electrode before and after spraying with carbon nanotubes and depositing of PECVD-carbon. As seen in the figure, after spraying, the top surface became smoother than the pre-sprayed surface (Figure 4a) and was covered fully with CNTs. It is seen that an adequate encapsulation layer could not be conformally deposited by PECVD without the sprayed CNT layer. The sprayed CNT layer was, therefore, a necessary precursor for the subsequent PECVD carbon layer. The areal mass of the CNT spray was about 0.15 ± 0.05 mg/cm^2 as measured by an electronic balance before and after spraying; the thickness was approximately 250–300 nm and was measured by SEM and Atomic Force Microscopy (AFM). The resultant areal mass of PECVD carbon was 0.12 ± 0.03 mg/cm^2, and the average layer thickness was 300 ± 10 nm. As shown in
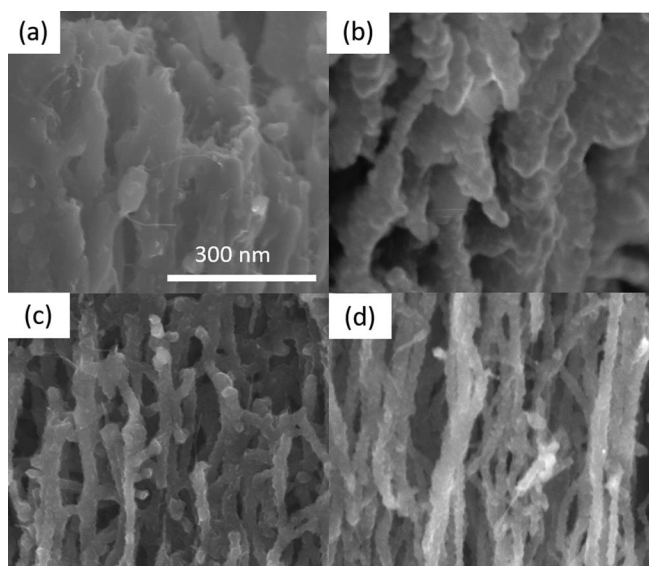

Figure 3. (a) Cross-section showing bare CNTs, (b) CNTs after 2 minutes of carbon infiltration, (c) CNTs after carbon infiltration and lightly loaded Si deposition ($\sim$1 vol%), and (d) CNTs after carbon infiltration and heavily loaded Si infiltration ($\sim$10 vol%). All SEM micrographs were taken at the same magnification.

Figures 4c and 4d, the PECVD appears to completely encapsulate the top surface.

Impact of cycling on electrode morphology.—Encapsulated electrodes were examined by SEM and EDS before and after cycling and compared with unencapsulated electrodes to determine the impact of encapsulation on the morphology of cycled electrodes. In particular, the effectiveness of the encapsulation layer for excluding the electrolyte from the silicon surface was assessed. The morphological differences of Si-VACNT electrodes after 20 galvanostatic cycles at C/10 were examined by SEM for unencapsulated and encapsulated electrodes with approximately 2% and 11% of silicon volume are shown in Figures 5 and 6, respectively. These figures show a dra-
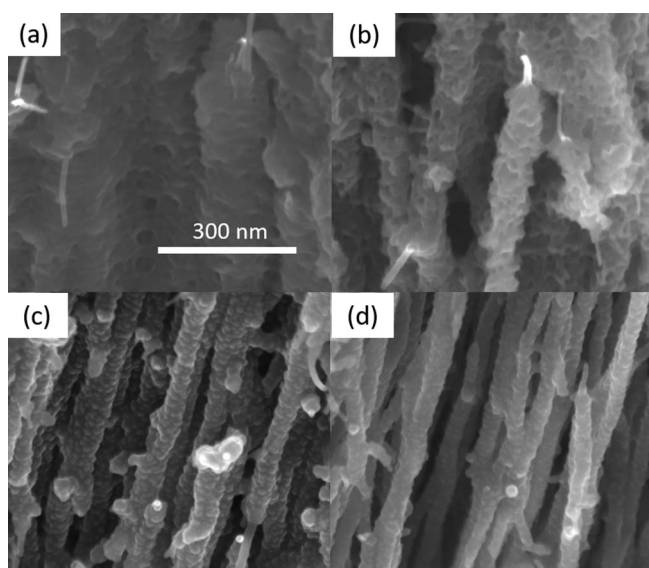

Figure 4. SEM micrographs of (a) top view of Si-VACNTs before encapsulation, (b) top view of Si-VACNT after spraying with CNTs, (c) top view of PECVD layer with CNT spray underneath, and (d) side view of Si-VACNTs after PECVD encapsulation.
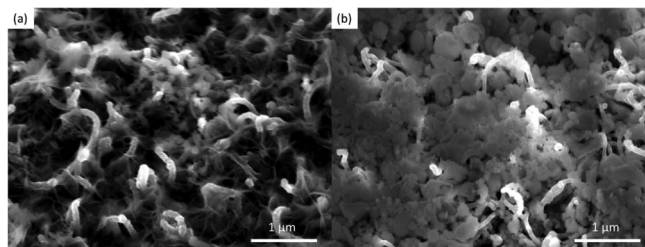
Figure 5. SEM micrographs showing cross-sectional views of cycled lightly loaded Si-VACNT electrodes without (a and b) and with (c and d) the encapsulation layer. The images on the left (a and c) were taken just underneath the top surface, while the images on the right (b and d) were taken 10 μm above the current collector.

matic morphological difference along the Si-VACNT electrodes. With the absence of the encapsulation layer, Si-VACNT electrode surfaces became rough and were covered with SEI products. In contrast, individual Si-VACNT tubes were still seen clearly when the encapsulation layer was present. The morphology of the silicon coating along the encapsulated Si-VACNT tubes did not change significantly from that of the uncycled electrodes (Figures 3c and 3d), even for heavily loaded silicon samples. It is evident that the encapsulation layer did make a difference on the Si-VACNT electrode surfaces, indicating that encapsulation was capable of blocking electrolyte solvents from entering into the Si-VACNT electrodes. Under such conditions, no appreciable SEI formation was observed on the silicon-coated tubes.

Figure 6. SEM micrographs showing cross-sectional views of cycled heavily loaded Si-VACNT electrodes without (a and b) and with (c and d) the encapsulation layer. The images on the left (a and c) were taken just underneath the top surface, while the images on the right (b and d) were taken 10 μm above the current collector.
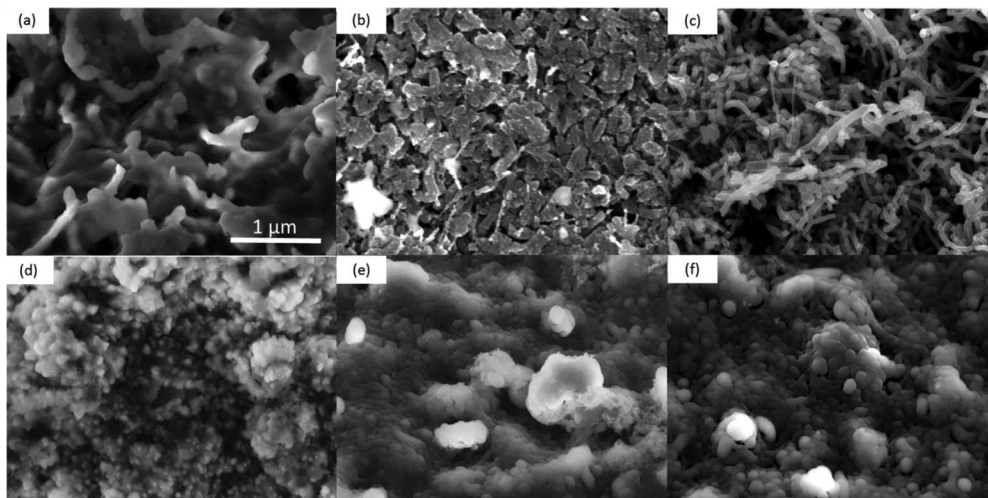

Figure 7. SEM micrographs showing morphological comparison of unencapsulated Si-VACNT electrodes cycled ten times at C/10 with (a) and without (b) FEC.

A few similar tests were performed to see how the electrolyte additive, FEC, impacted the surface morphology of unencapsulated Si-VACNT electrodes. As seen in Figure 7, there was a significant difference in the morphology of the top surface due to the FEC additive, with much less SEI formed in the presence of FEC. Previous studies proposed that FEC-containing electrolytes stabilize the SEI by forming a polyfluorocarbonate on the surface, which lowers charge-transfer resistance and promotes Li transport.[23] The observation of significantly less SEI formation in the presence of FEC is consistent with this explanation.

Figure 8 shows SEM images of the top surface of both unencapsulated and encapsulated Si-VACNT electrodes before/after an ethylene carbonate wash and after SEI removal. All the electrodes had been cycled five times at C/10. The electrolyte used in these tests did not contain FEC. As seen in Figures 8a and 8d, the top surfaces were covered with a thick SEI layer and perhaps with some residual electrolyte. Small granules were observed in the layer formed on the encapsulated electrode. After washing in EC, the unencapsulated surface still showed considerable SEI products (Figure 8b), while the encapsulated surface was much smoother (Figure 8e). From these images, it appears that the SEI formed on the unencapsulated electrode was thicker than that on the encapsulated electrode. After an acid rinse (Figures 8c and 8f), both top surfaces were similar to their pre-cycled geometry (Figures 4a and 4c), and the encapsulation layer was still intact. The differences observed between the SEI formed on the encapsulated layer (made out of carbon) and that formed on the silicon surface of unencapsulated electrodes are consistent with the literature.[24]

The morphological differences observed between the cycled encapsulated and unencapsulated electrodes should also be reflected in the local composition of the electrodes. According to the literature, LiF and Li_2CO_3 are two primary constituents of the SEI.[4,25] The electrolyte itself also contains fluorine. Therefore, the content of fluorine and oxygen should be impacted by the presence of the SEI. Figure 9 shows SEM/EDS characterization results for electrodes both with and without encapsulation. Measurements were taken at multiple locations (as indicated in Figure 9a) along the electrodes before cycling and after 100 cycles at C/10. The mass fractions of fluorine and oxygen relative to silicon are shown in Figures 9b and 9c, respectively. The data for electrodes prior to cycling and without washing in the solvent are included to assess the extent, if any, to which the electrolyte is able to penetrate the electrode structure underneath the encapsulation layer during the 12-hour (minimum) soak period before the initiation of cycling. As indicated in Figures 9b and 9c, both the fluorine and oxygen fractions were much higher for the unencapsulated electrodes, consistent with effective blocking of the electrolyte by the encapsulation layer. There was, however, a relatively small amount of electrolyte in the Si-VACNT structure prior to cycling, as indicated by the small amount of F measured below the encapsulation layer. Even so, there was no evidence for continued electrolyte penetration since the amount did not change during cycling. It appears that encapsulated electrodes are likely "sealed" by the SEI from further electrolyte penetration. The lower apparent fluorine amount at the top of the unencapsulated electrode is believed to be the result

Figure 8. SEM micrographs of unencapsulated (a-c) and encapsulated (e-f) Si-VACNT electrode top surfaces following 5 cycles at C/10: at the end of the test (a, d); after washing with ethylene carbonate (b, e); and after SEI removal (c, f).

of more silicon (rather than less fluorine) at the top of the electrode due to non-uniform silicon deposition, coupled with normalization by silicon. The results for oxygen were similar to those of fluorine.

A TEM line scan was also performed on tubes from an encapsulated electrode with 12 vol% of silicon. Although the TEM results are obviously localized to the specific tube(s) analyzed, no statistically significant fluorine was detected and there was no evidence for SEI formation on the surface as shown in Figure 10. In addition, the oxygen composition tracked that of the silicon and is most likely due to the native oxide layer on the silicon surface. The oxygen composition did not follow that of the carbon as would be expected for Li_2CO_3. In contrast, the additional oxygen shown for the unencapsualted Si-VACNT electrodes (Figure 9c) may be associated with Li_2CO_3, a SEI formation product.

Finally, an approximate "drop test" was performed, in addition to the analysis results described above. Several drops of electrolyte were placed onto the top surface of encapsulated and unencapsulated electrodes and observed. The electrolyte on the unencapsulated electrodes was observed to soak into the electrode. In contrast, the electrolyte on the encapsulated electrodes appeared to remain on the surface and eventually evaporate, leaving a salt residue.
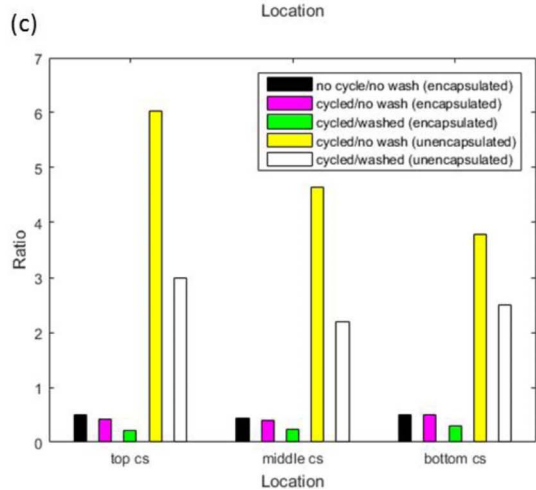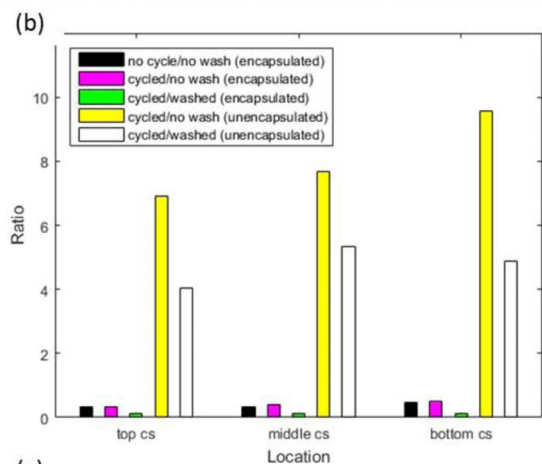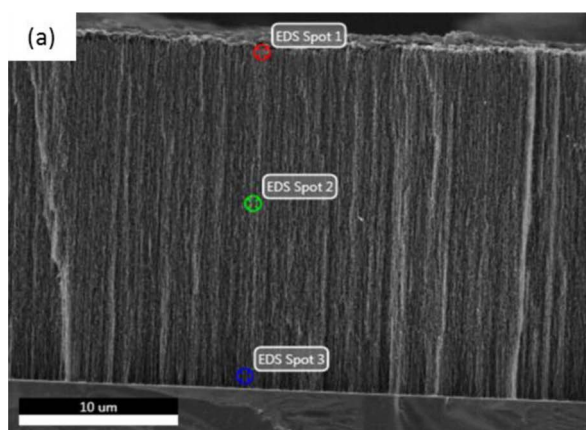
Taken together, the composition results are consistent with the morphological results presented above, and reflect the lack of significant SEI formation for the encapsulated electrode. The addition of FEC as an electrolyte additive also decreased SEI formation to some extent. Having established the impact of encapsulation on the morphology and local composition of the Si-VACNT electrode, we now examine its impact on electrode performance.

Electrochemical characterization.—*Impact of encapsulation and different C-rates on cycling performance.*—Electrodes were cycled at two different C-rates both with and without encapsulation in order to determine the impact of encapsulation on cell performance. Figure 11 presents galvanostatic cycling results for electrodes cycled without FEC at C/10 (a-c) and C/2 (d-e), where capacity is plotted as a function of cycle number. The specific capacities were normalized by the method described previously (Electrochemical characterization section). The capacity fade for both types of electrodes increased with increased Si loading as shown in Figure 11. In spite of the encapsulation layer and independent of C-rate, the cycling performance of lightly and medium-loaded electrodes was similar. The similar performance of these electrodes indicates that SEI formation was not the primary cause of capacity fade. A slight improvement due to encapsulation was observed for the heavily loaded electrodes, although the capacity fade for these electrodes was quite pronounced. Again, given

the documented dramatic reduction in SEI formation for encapsulated electrodes, one would have expected a dramatic difference in cycling performance if unstable SEI formation at the silicon interface were the primary cause of capacity fade.

Further insight into capacity fade for these electrodes was obtained by observing the condition of the electrodes after cycling. It was found that, independent of encapsulation, heavily loaded electrodes literally fell apart when removed after cycling 30–40 times, whereas electrodes with a lower silicon loading did not. Microscopic examination of encapsulated electrodes provided additional understanding by allowing us to observe the impact of cycling on the encapsulation layer. As shown in Figure 12a, after SEI removal, the encapsulation layer for an electrode containing 6 vol% silicon was essentially intact after 50 cycles, although some cracking was observed. However, pronounced cracking was observed after 100 cycles, and the encapsulation layer was completely fragmented in Figure 12b. The same types of changes occurred much sooner for electrodes with a higher silicon fraction (see Figures 12c and 12d). Thus, for our electrodes, at least an element of the volume expansion appeared to be cumulative, and rapid capacity fade leading to failure was associated with mechanical disintegration of the electrode, probably directly related to separation of active material from the current collector. Figure 13 is a lower magnification image of a section of a failed heavily loaded electrode, and illustrates the severe structural degradation that can occur. In this extreme case, pieces that were detached from or poorly attached to the electrode surface were disrupted during the disassembly of the cell. This observation was unexpected since the nanostructure of the electrode seemed to contain more than adequate space for silicon expansion. Similar behavior was observed for unencapsulated electrodes, which also degraded mechanically after similar numbers of cycles.
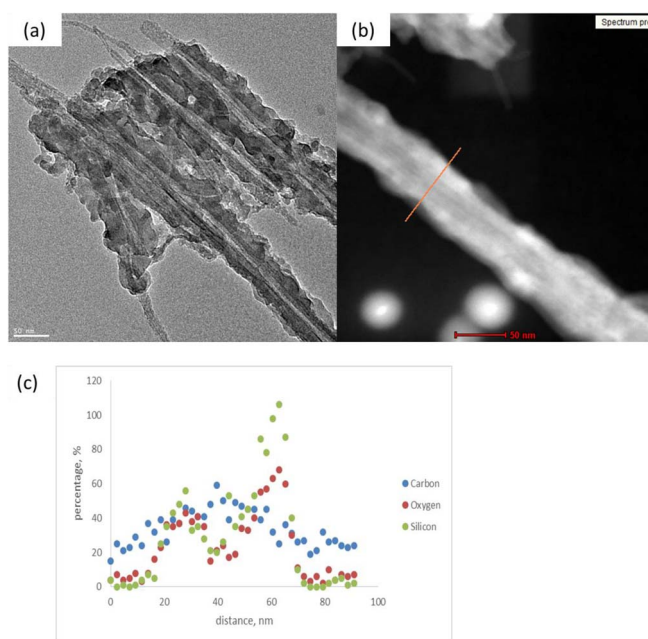
Coulombic efficiency.—The impact of the encapsulation layer on the Coulombic efficiency (CE) was also examined. The CE values that correspond to the cycling performance in Figure 11 are summarized in Table I for the initial cycle and after 30 cycles at C/10. The initial CE values increased with increasing silicon volume fraction and were relatively low; in contrast, the values after 30 cycles were significantly higher and decreased slightly with increasing Si volume fraction. In all cases, the CE values for encapsulated electrodes were greater than those measured for unencapsulated electrodes under similar conditions. Low values for the coulombic efficiency have been attributed to irreversible losses associated with SEI formation. However, if SEI formation on Si were the primary cause of the low CE values, then a greater difference between the encapsulated and unencapsulated electrodes might have been expected, in light of the significant differ-

Figure 10. TEM micrographs of (a) Si-VACNTs and (b) a single Si-VACNT where a line scan was performed. The orange line in (b) indicates the location of line scan. (c) shows the line-scan spectrum of C, O and Si.

Figure 9. (a) SEM micrograph showing three locations for EDS characterization. (b) Fluorine content normalized by the associated silicon at those locations. (c) Oxygen content normalized by the silicon content. The analyses in (b) and (c) were performed for electrodes at five different conditions: i) not cycled and no solvent wash (encapsulated), ii) cycled/no wash (encapsulated), iii) cycled/washed (encapsulated), iv) cycled/no wash (unencapsulated), and v) cycled/washed (unencapsulated), respectively.

ence in SEI formation observed microscopically for the two types of electrodes.
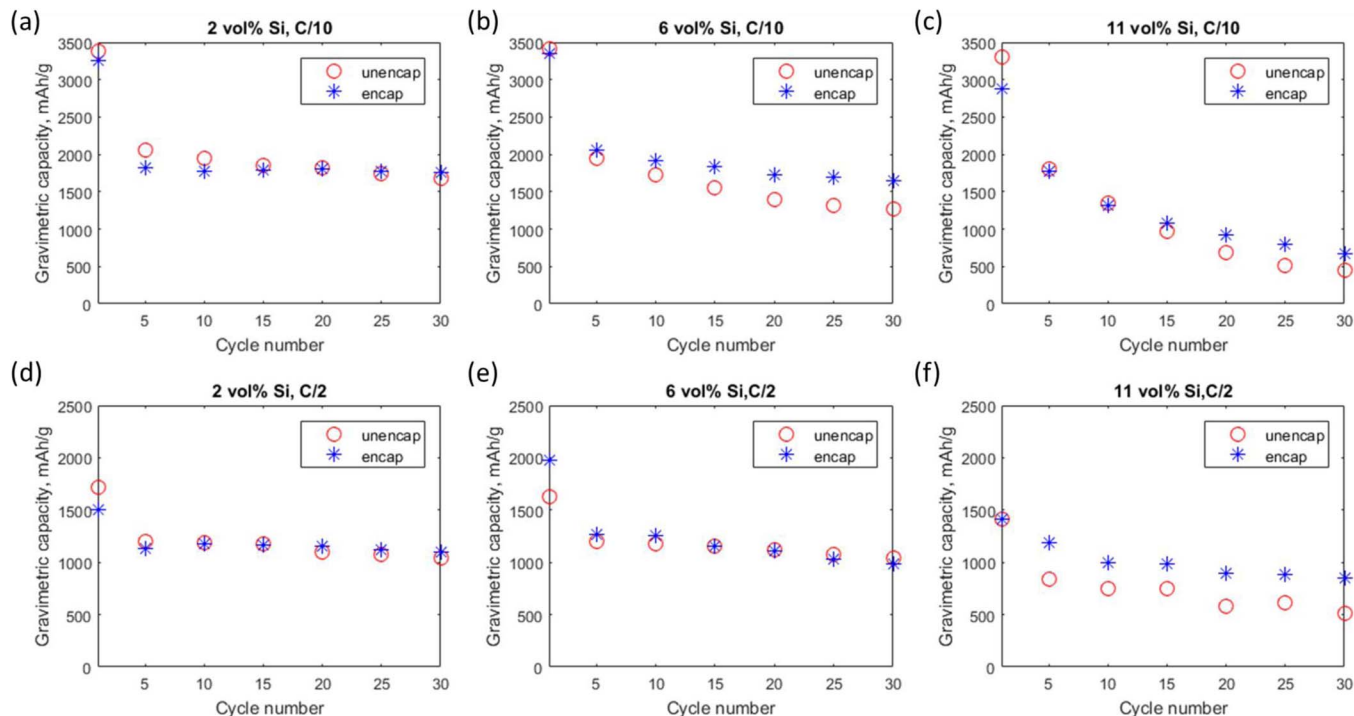
Impact of encapsulation and FEC electrolyte additive.—Recently, FEC has been used as an electrolyte additive for silicon-based electrodes to improve cycling performance. Consequently, a few experiments with encapsulated electrodes were performed to learn more regarding the role of the FEC. Both lightly (∼2 vol%) and heavily loaded (∼11%) encapsulated electrodes were cycled at C/10 in an

electrolyte containing 10 wt% FEC (see Figure 14). It was observed that encapsulated electrodes with FEC had an initial capacity similar to that observed without FEC. Therefore, FEC did not impact significantly the processes responsible for the initial drop in capacity in encapsulated electrodes. However, lightly loaded electrodes with FEC showed a slightly higher capacity for the first twenty cycles. This is consistent with an SEI layer that is less resistive in the presence of FEC. After twenty cycles, the capacity was similar for electrodes both with and without FEC, presumably to the consumption of FEC as discussed in the literature.[26] Since encapsulation precludes the formation of unstable SEI at a silicon/electrolyte interface by preventing the electrolyte from contacting the silicon, the effect of FEC in our experiments must be due to processes that take place at the interface between the encapsulation layer (carbon) and the electrolyte. Heavily loaded electrodes with FEC still experienced pronounced fading, but their capacity was higher than that of the electrodes without FEC. The capacity difference was most pronounced for the early cycles, and is also consistent with the consumption of FEC during cycling.[26] We note that the superficial current density was higher for the heavily loaded electrodes at the same C/10 rate, and it is likely that this influenced the impact of the FEC on the capacity since the encapsulation layer was essentially the same. Finally, although FEC did impact the capacity of our encapsulated electrodes, it did not appear to enhance the lifetime of encapsulated electrodes, especially for the heavily loaded electrodes. The principal mechanism responsible for electrode failure (or the lack thereof) for the range of conditions examined in our experiments is apparently not the result of SEI formation.
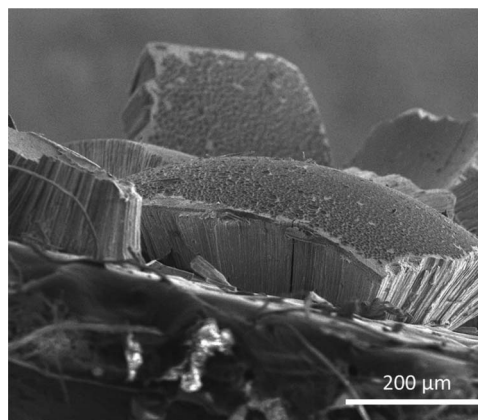
To this point, we have examined the impact of a PECVD encapsulation layer on SEI formation and electrode performance. This layer significantly reduces SEI formation and appears to effectively prevent the electrolyte from directly contacting the Si-coated VACNTs. However, the large reduction in SEI formation does not prevent the Si-VACNT electrodes used in this study from fading. Also, surprisingly, the overall performance of encapsulated and unencapsulated electrodes is similar, in spite of the large difference in the amount of SEI formed in the two types of electrodes, and significant differences in the type of transport that takes place. The ability to get lithium into and out of the electrode is critical, and the VACNT geometry
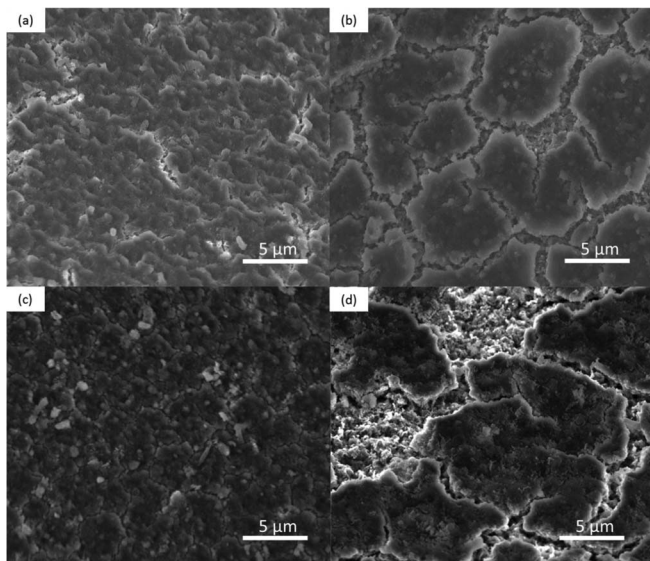
Figure 11. Comparison of unencapsulated and encapsulated Si-VACNT electrodes with various silicon volume fractions cycled at C/10 (a-c) and C/2 (d-f). The capacities are lithiation capacities. Cells were cycled without FEC.

is ideally suited for study of lithium transport in the presence of the encapsulation layer, as described in the next section.

Li transport in encapsulated Si-VACNTs.—As demonstrated previously, the implementation of an encapsulation layer inhibited the SEI formation in the Si-VACNT electrodes; thus, the physical environment differed significantly from that of the unencapsulated electrodes. In particular, the lack of electrolyte in the electrode underneath the encapsulation layer altered transport in the electrode. Prior to exam-

Figure 13. SEM micrograph of a failed, heavily loaded electrode showing structural degradation. The fragments in the image that were separated from the current collector may have been disrupted during disassembly of the cell.
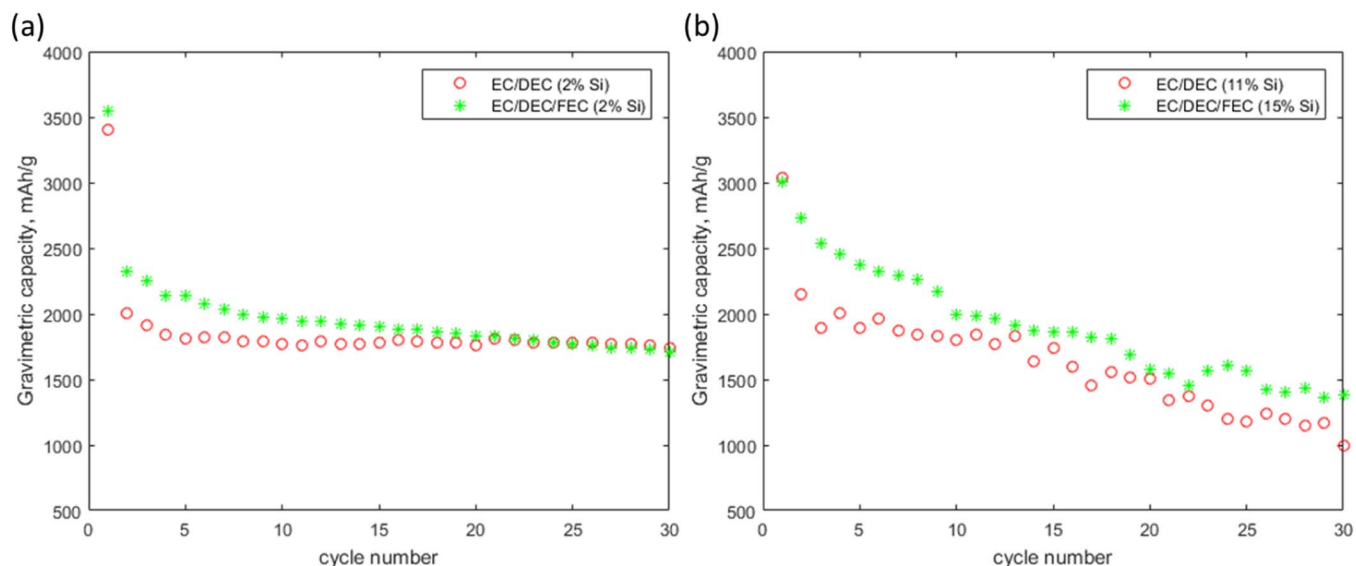

Figure 12. SEM micrographs of the encapsulation layers of a lightly loaded (~6%) electrode after (a) 50 cycles and (b) 100 cycles and the encapsulation layer of a heavily loaded electrode (~15 vol%) after (c) 20 cycles and (d) 40 cycles.

Table I. Comparison of Coulombic efficiency for Si-VACNT electrodes cycled at C/10 and C/2 with and without the encapsulation layer.

| | C/10 | | | |
| | Unencapsulated | | Encapsulated | |
Si volume fraction	Initial CE (%)	CE After 30 cycles (%)	Initial CE (%)	CE After 30 cycles (%)
2%	50 ± 12.3	97 ± 1.1	59 ± 3.9	98 ± 2.5
6%	67 ± 2.9	96 ± 0.7	71 ± 5.8	95 ± 4.2
11 %	69 ± 6.9	93 ± 1.2	72 ± 1.7	95 ± 1.8

(a)

(b)

Figure 14. Cycling comparison between encapsulated electrodes with and without FEC.

ining this further, capacitance data were taken to confirm the lack of an electrolyte path for lithium-ion transport in these electrodes. Results are shown in Table II for both encapsulated and unencapsulated electrodes. As seen in the table, the capacitance of the unencapsulated cells is significantly higher than that of the encapsulated cells. This is consistent with exposure to a much larger surface area. The surface area, and hence the capacitance, changes with height (electrode thickness) for unencapsulated electrodes as would be expected. In contrast, the capacitance of the encapsulated electrodes was much lower, in agreement with a lower contact area between the electrolyte and the electrode. Finally, and importantly, the capacitance of the encapsulated cells did not vary with tube height. These results are consistent with and provide additional evidence for a lack of electrolyte path to tubes below the encapsulation layer.

The absence of an electrolyte path in the nanotube forest precludes the transport of lithium ions through the liquid phase to the silicon surface in the electrode beneath the encapsulation layer. That transport must occur along the tubes themselves in these electrodes, and it is the purpose of this section to explore in greater detail its impact on battery performance. To do so, experiments were performed on encapsulated electrodes of different heights. Two types of experiments were performed on these electrodes: 1) experiments at the same C-rate, and 2) experiments at the same superficial current density (current per cross-sectional area of the cell). These experiments were performed at different C-rates for several silicon loadings.

Figure 15 shows the cycling results (10 cycles) at different C-rates and silicon loadings for electrodes with heights that ranged from 60 µm to ~200 µm. Of these, the electrodes with a height of ~ 90 µm were compared previously to unencapsulated electrodes and found to

behave similarly. The results in Figure 15 show that electrodes with the same silicon volume fraction had similar gravimetric capacities, independent of height. The lack of height-related performance indicates that lithium transport along the tubes in the height direction (perpendicular to the current collector) does not limit battery performance. This is especially significant when the aspect ratio of the tube is taken into account. The typical silicon thickness is about 25 nm, while the tube height is on the order of 100 µm, a difference of more than four orders of magnitude.

It is helpful to consider the results of Figure 15 in the light of factors that may limit battery behavior. For encapsulated cells, these factors include resistances that scale with the superficial current density such as the separator resistance, the resistance to lithium transport through the encapsulation layer, or resistance associated with the lithium metal counter electrode. For a given C-rate and silicon volume fraction, these resistances should be greater for the taller electrodes, which have a higher superficial current density. This follows from the fact that the taller electrodes have more silicon and, therefore, a greater absolute capacity and a higher current at a specified C-rate. The observation that the taller electrodes do not perform less effectively (see Figure 15) indicates that these "superficial" resistances do not limit battery performance under the conditions tested.
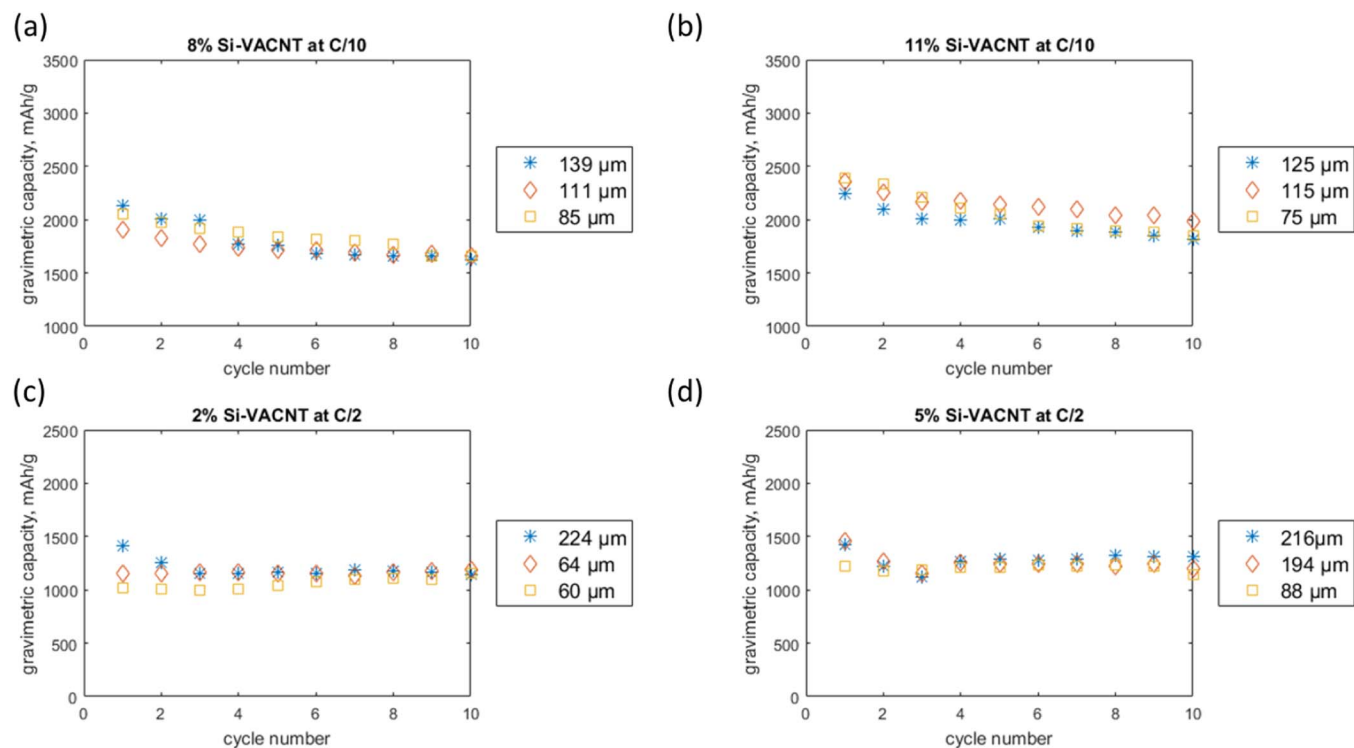
Additional factors that may limit battery performance include the transport of lithium in the Si-VACNT electrode in either the tube direction (direction of current flow) or the radial direction. We will refer to these as the resistances associated with transport "along" the tubes and transport "into" the tubes. If transport along the tubes were limiting, battery performance would be expected to depend strongly on electrode height, and lithium would tend to fill the electrode from the top down during charging. The higher superficial current associated with the taller electrodes would further degrade performance and accentuate height-related performance limitations. In contrast, if transport into the silicon were limiting, the lithium would have essentially equal access to the silicon along the length of the tube and height-related performance degradation would not be observed. Under such conditions, the gravimetric capacity of the electrode would be independent of height. The results shown in Figure 15 are consistent with limitation by transport "into" the tubes.

The conclusion that transport into the tubes is limiting has important implications. Given the very high aspect ratio of the tubes, the distance along the tubes from the top to the bottom of the electrode is orders of magnitude larger than the radial distance. Therefore, the rate of transport along the tubes must be orders of magnitude faster than the rate of transport in the radial direction. For that to be the case,

Table II. Capacitance of unencapsulated and encapsulated electrodes after 100 cycles at C/10.

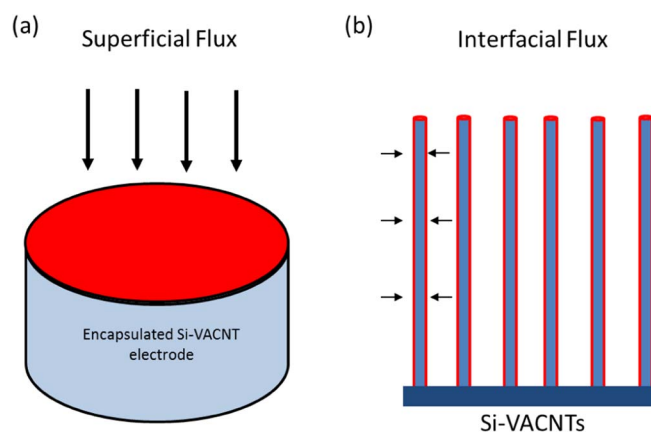| Cell #	Encapsulated	Electrode Height (µm)	Capacitance (µF)
1	No	37	62
2	No	84	113
3	No	98	185
4	No	135	258
5	Yes	73	3.4
6	Yes	127	2.7
7	Yes	130	3.9

Figure 15. Performance of encapsulated Si-VACNT electrodes of various heights cycled at C/10 (a-b) and C/2 (c-d).

the mechanisms by which lithium enters or leaves the silicon lattice must be very different from the mechanisms that determine the transport rate along the tubes. It is likely that surface diffusion dominates transport along the tube length.
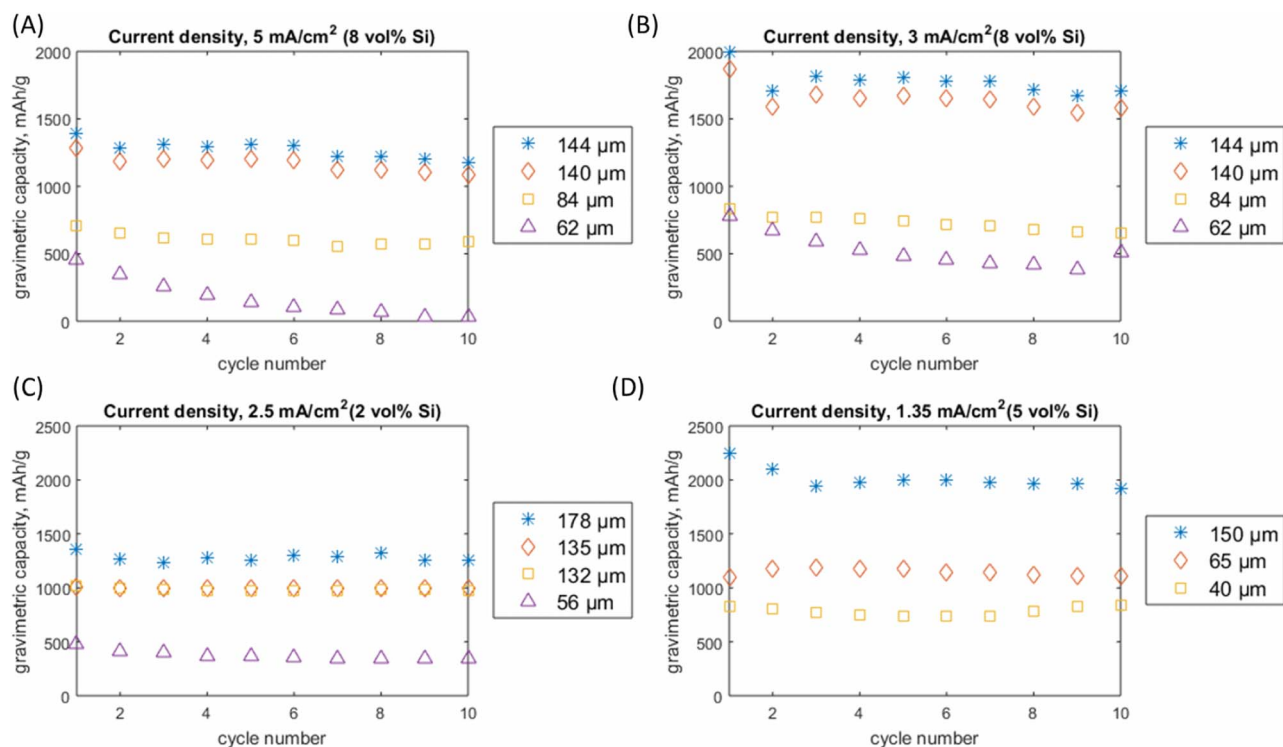
It appears that the tall electrodes may have performed slightly better than the short electrodes for the first few cycles at C/2. These cycles were preceded by two conditioning cycles at C/10, as described in the procedure section. Cycling at a higher C-rate does impact voltage losses in the cell, but these losses would favor shorter electrodes as noted above. The higher early-cycle capacity of the taller electrodes has not yet been explained mechanistically, and is the subject of continuing investigation.

The above experiments can be used to provide important insight into the speed at which the lithium is able to move along the length of the silicon-coated nanotubes. In order to avoid limitations due to transport in the height direction, consistent with our experimental observations, lithium would, as a minimum, need to traverse the entire distance from the top to the bottom of the electrode (e.g., the height) during the length of the experiment (e.g., time required to charge the electrode). Considering just the tallest electrode (224 μm) and shortest charge time (3621 sec) in order to estimate a minimum velocity, lithium must travel a minimum of 61 nm/s. This value is comparable to results from the in-situ microscopic study of McDowell et. al,[27] where an average rate of ∼69 nm/sec along silicon nanowires was observed. It is likely that the velocities in our system are significantly higher than 60 nm/s, since lithium that just barely arrives at the bottom of the electrode at the end of the experiment would not have time to be incorporated into the silicon, which incorporation is the slower process. Given the absence of height limitations in our experiments, a more reasonable estimate of the speed would assume that the lithium was able to traverse the entire electrode height in a fraction, say 10%, of the total charge time, yielding an estimated velocity of ∼600 nm/s. Thus, the lack of observed height limitations in our experiments requires a minimum speed of ∼60 nm/s, but is more consistent with speeds that are an order of magnitude faster.

Experiments were also performed at a constant superficial current density in order to confirm the observations made at constant C-rate, and to provide additional insight into the factor(s) that limit electrode performance. As illustrated in Figure 16, the superficial current density is the applied current normalized by the entire cross-sectional area of an encapsulated electrode, which was 1 cm². In contrast, the interfacial current density is the applied current normalized by the total surface area of silicon-coated nanotubes. Four different superficial current densities were examined at different silicon loadings as shown in Figure 17. In general, performance improved with decreasing current density as expected. However, in contrast to the previous results, tests performed at the same superficial current density showed a clear increase in capacity with increasing electrode height. In other words, the tall electrodes performed better than their shorter counterparts.

Figure 16. Schematic diagram showing (a) the superficial flux and (b) the interfacial flux. The areas that define the corresponding fluxes are highlighted in red.
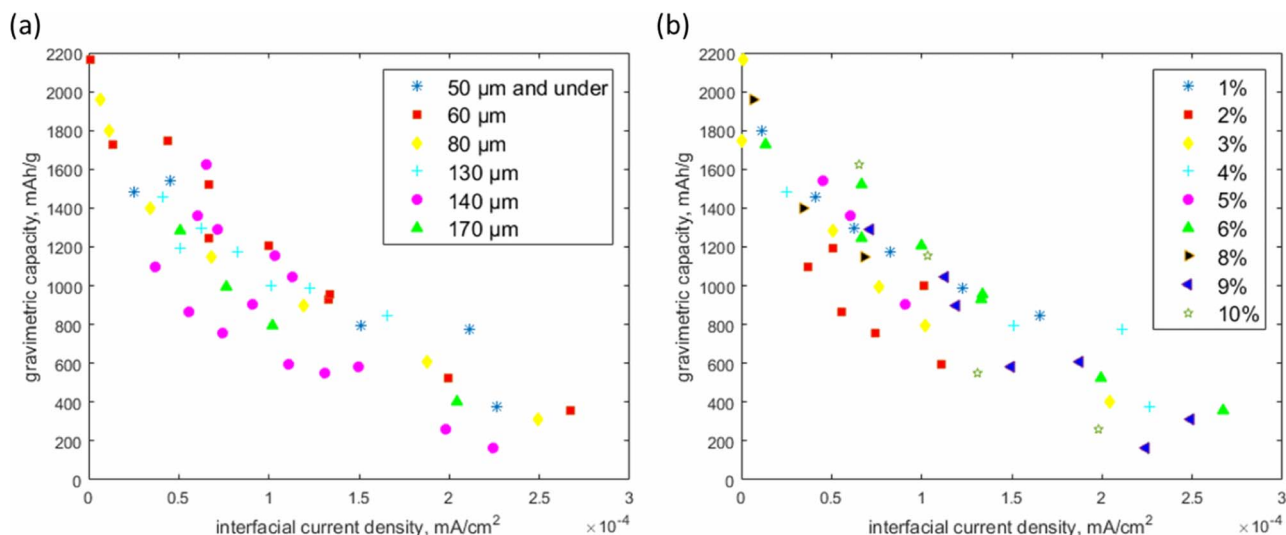
Figure 17. Cycling results for encapsulated Si-VACNT electrodes of various heights cycled at the specified superficial current densities.

This, of course, is the opposite of what one would expect if transport along the tubes were limiting, consistent with the results above.

The improved performance of the tall electrodes at a given superficial current density can be explained in terms of the surface area of the tubes, and is consistent with a process controlled by radial transport between the inside and outside of the tubes. Let's consider charging for the moment, although similar arguments apply to the discharge process. Tests at a constant superficial current density result in a constant absolute rate of lithium insertion into the Si electrode. The surface area over which that insertion can take place is greater for the taller electrodes; therefore, the insertion rate per tube surface area (interfacial area) is lower for those electrodes. This results in better relative performance.

Figure 18 summarizes the relationship between the gravimetric capacity and interfacial current density, which is the current divided by the actual surface area of the nanotubes. Tests performed at a variety of electrode heights ranging from 40 μm to 170 μm as indicated in Figure 18a. No trend with height is apparent. However, there is a clear and strong relationship between the capacity and the interfacial current density. These tests also span a range of silicon volume fractions as shown in Figure 18b. Again, no clear trend is observed with respect to the volume fraction, but the capacity is a strong function of the interfacial current. The correlation of the capacity with the interfacial current density is an important finding of the present study, and describes results for a range of electrode heights, silicon volume fractions and C-rates. In all cases, the gravimetric capacity

Figure 18. Dependence of electrode capacity on the interfacial current density for electrodes of different heights and silicon loadings. (a) symbols indicate electrode height, and (b) symbols indicate silicon volume fraction.

of the electrodes depends strongly on the interfacial current density during charge, which is consistent with behavior that is limited by radial transport into the tubes rather than transport along the length of the tubes.

Conclusions

This study examined the impact of encapsulation on the performance of Si-VACNT electrodes. Use of an encapsulation layer was shown to prevent SEI formation on the high-surface- area silicon electrode formed on a template of vertically aligned carbon nanotubes. A comparison of encapsulated and unencapsulated electrodes revealed large differences in the morphology and composition of the electrodes due to encapsulation. These large differences, however, were not reflected in the results from electrochemical testing, which were relatively similar for the two types of electrodes (encapsulated and unencapsulated) at different silicon loadings and C-rates. Capacity fade was still observed for encapsulated electrodes, and their performance relative to that of unencapsulated electrodes indicates that SEI formation, which was very different for the two electrodes, was not the primary factor affecting cycle life. Morphology changes during cycling indicate that aspects of the volume change are cumulative, and eventually create large mechanical stresses, even in these nanostructured electrodes.

Encapsulation altered the transport of lithium in the Si-VACNT electrodes, and experiments were performed to help understand the factors that govern lithium transport in the absence of electrolyte. Two different transport directions and length scales are relevant–1) radial transport of Li in/out of each silicon-coated nanotube ($\sim$50 nm diameter) and 2) lithium transport along the length of the nanotubes ($\sim$100 μm height). Experimental results indicate that the height of the Si-VACNT electrodes does not limit Li transport, even though that height was orders of magnitude greater than the diameter of the tubes. In fact, taller electrodes exhibited a higher normalized (gravimetric) capacity than shorter electrodes at a given current. The overall performance of the electrodes scaled with the silicon surface area. These results have important implications for a variety of encapsulation strategies.

Acknowledgment

References

1. J. Li and J. R. Dahn, *Journal of The Electrochemical Society*, **154**, A156 (2007).
2. G. C. L. B. A. Boukamp and R. A. Huggins, *Journal of Electrochemical Society*, **128**, 725 (1987).
3. M. N. Obrovac and L. J. Krause, *Journal of The Electrochemical Society*, **154**, A103 (2007).
4. Y. M. Lee, J. Y. Lee, H.-T. Shim, J. K. Lee, and J.-K. Park, *Journal of The Electrochemical Society*, **154**, A515 (2007).
5. C. K. Chan, R. Ruffo, S. S. Hong, R. A. Huggins, and Y. Cui, *Journal of Power Sources*, **189**, 34 (2009).
6. Q. Zhang, W. Zhang, W. Wan, Y. Cui, and E. Wang, *Nano Lett*, **10**, 3243 (2010).
7. W. Xu, S. S. S. Vegunta, and J. C. Flake, *Journal of Power Sources*, **196**, 8583 (2011).
8. V. Chakrapani, F. Rusli, M. A. Filler, and P. A. Kohl, *The Journal of Physical Chemistry C*, **115**, 22048 (2011).
9. G. Chan, J. W. Choi, I. Ryu, Y. Yao, M. T. McDowell, S. W. Lee, A. Jackson, Y. Yang, L. Hu, and Y. Cui, *Nat Nanotechnol*, **7**, 6p (2012).
10. R. R. Li-Feng Cui, Candace K. Chan, Hailin Peng, and Yi Cui, *Nano Lett*, **9**, 491 (2009).
11. L. Su, Y. Jing, and Z. Zhou, *Nanoscale*, **3**, 3967 (2011).
12. Y. Fan, Q. Zhang, C. Lu, Q. Xiao, X. Wang, and B. K. Tay, *Nanoscale*, **5**, 1503 (2013).
13. J.-L. Zang and Y.-P. Zhao, *Composites Part B: Engineering*, **43**, 76 (2012).
14. W. Wang, R. Epur, and P. N. Kumta, *Electrochemistry Communications*, **13**, 429 (2011).
15. K. Evanoff, J. Khan, A. A. Balandin, A. Magasinski, W. J. Ready, T. F. Fuller, and G. Yushin, *Adv Mater*, **24**, 533 (2012).
16. Y. Oumellal, N. Delpuech, D. Mazouzi, N. Dupré, J. Gaubicher, P. Moreau, P. Soudan, B. Lestriez, and D. Guyomard, *Journal of Materials Chemistry*, **21**, 6201 (2011).
17. N. Liu, H. Wu, M. T. McDowell, Y. Yao, C. Wang, and Y. Cui, *Nano Letters*, **12**, 3315 (2012).
18. N. Liu, Z. Lu, J. Zhao, M. T. McDowell, H.-W. Lee, W. Zhao, and Y. Cui, *Nat Nano*, **9**, 187 (2014).
19. M. Ashuri, Q. He, and L. L. Shaw, *Nanoscale*, **8**, 74 (2016).
20. R. Yi, J. Zai, F. Dai, M. L. Gordin, and D. Wang, *Nano Energy*, **6**, 211 (2014).
21. J. Song, Fabrication and application of vertically aligned carbon nanotube templated silicon nanomaterials, in *Physics Department*, Brigham Young University, Provo (2011).
22. A. D. Willey, J. M. Holt, B. A. Larsen, J. L. Blackburn, S. Liddiard, J. Abbott, M. Coffin, R. R. Vanfleet, and R. C. Davis, *Journal of Vacuum Science & Technology B*, **32**, 011218 (2014).
23. K. Schroder, J. Alvarado, T. A. Yersak, J. Li, N. Dudney, L. J. Webb, Y. S. Meng, and K. J. Stevenson, *Chemistry of Materials*, **27**, 5531 (2015).
24. Y.-C. Yen, S.-C. Chao, H.-C. Wu, and N.-L. Wu, *Journal of The Electrochemical Society*, **156**, A95 (2009).
25. C. K. Chan, R. Ruffo, S. S. Hong, and Y. Cui, *Journal of Power Sources*, **189**, 1132 (2009).
26. R. Jung, M. Metzger, D. Haering, S. Solchenbach, C. Marino, N. Tsiouvaras, C. Stinner, and H. A. Gasteiger, *Journal of The Electrochemical Society*, **163**, A1705 (2016).
27. M. T. McDowell, S. Woo Lee, C. Wang, and Y. Cui, *Nano Energy*, **1**, 401 (2012).